Research Article

Image Restoration Based on the Hybrid Total-Variation-Type Model

Baoli Shi,[1] Zhi-Feng Pang,[1, 2] and Yu-Fei Yang[3]

[1] *College of Mathematics and Information Science, Henan University, Kaifeng 475004, China*
[2] *Division of Mathematical Sciences, School of Physical and Mathematical Sciences, Nanyang Technological University, Singapore 637371*
[3] *Department of Information and Computing Science, Changsha University, Changsha 410003, China*

Correspondence should be addressed to Zhi-Feng Pang, zhifengpang@163.com

We propose a hybrid total-variation-type model for the image restoration problem based on combining advantages of the ROF model with the LLT model. Since two L^1-norm terms in the proposed model make it difficultly solved by using some classically numerical methods directly, we first employ the alternating direction method of multipliers (ADMM) to solve a general form of the proposed model. Then, based on the ADMM and the Moreau-Yosida decomposition theory, a more efficient method called the proximal point method (PPM) is proposed and the convergence of the proposed method is proved. Some numerical results demonstrate the viability and efficiency of the proposed model and methods.

1. Introduction

Image restoration is of momentous significance in coherent imaging systems and various image processing applications. The goal is to recover the real image from the deteriorated image, for example, image denoising, image deblurring, image inpainting, and so forth; see [1–3] for details.

For the additive noisy image, many denoising models have been proposed based on PDEs or variational methods over the last decades [1–3]. The essential idea for this class of models is to filter out the noise in an image while preserving significant features such as edges and textures. However, due to the ill-posedness of the restoration problem, we have to employ some regularization methods [4] to overcome it. The general form of regularization methods consists in minimizing an energy functional of the following form:

$$F(\overline{u}) = \frac{\lambda}{2}\|\overline{u} - \overline{u}_0\|_{\mathcal{X}}^2 + \mathcal{R}(\overline{u}) \tag{1.1}$$

in Banach space $\mathcal{X}$, where λ is the regularization parameter, $\mathcal{R}$, is a regularization term, $\overline{u}_0$ is the observed image, and $\overline{u}$ is the image to be restored. The development of the energy functional (1.1) actually profits from the ROF model [5] which is of the following form:

$$\min_{\overline{u}} \frac{\lambda_1}{2} \|\overline{u} - \overline{u}_0\|_{L^2}^2 + |\overline{u}|_{BV}, \tag{1.2}$$

where $|\overline{u}|_{BV} := \int_\Omega |\nabla \overline{u}| \mathrm{d}x$. In the case without confusion, for simplification we omit the open set Ω with Lipschitz boundary for $\|\cdot\|_{L^2(\Omega)}$ and $|\cdot|_{L^1(\Omega)}$. Due to edge-preserving property of the term $|\overline{u}|_{BV}$, this model has been extended to other sorts of image processing problems such as

$$\min_{\overline{u}} \frac{\lambda_2}{2} \|K\overline{u} - \overline{u}_0\|_{L^2}^2 + |\overline{u}|_{BV} \tag{1.3}$$

for image deblurring [6] and

$$\min_{\overline{u}} \frac{\lambda_3}{2} \|\overline{u} - \overline{u}_0\|_{L^2(\Omega \setminus D)}^2 + |\overline{u}|_{BV} \tag{1.4}$$

for image inpainting [2, 7], where K is a blurring operator and D is the inpainting domain. Furthermore, this model was applied to restore the multiplicative noisy image which usually appears in various image processing applications such as in laser images, ultrasound images [8], synthetic aperture radar (SAR) [9], and medical ultrasonic images [10]. One of the models based on BV was proposed by Huang et al. (HNW) [11] with the form

$$\min_z \alpha \int_\Omega (z + fe^{-z}) \mathrm{d}x + |z|_{BV}, \tag{1.5}$$

where z is the logarithmic transformation of u and $|z|_{BV}$ keeps the total variation property related to $|e^z|_{BV}$ and $\alpha > 0$. Here u satisfies $f = u\eta$ for the noise η.

However, as we all know the $|\cdot|_{BV}$ term usually reduces the computational solution of the above models to be piecewise constant, which is also called the staircasing effect in smooth regions of the image. The staircase effect implies to produce new edges that do not exist in the true image so that the restored image is unsatisfactory to the eye. To overcome this drawback, some high-order models [12–15] have been proposed such as a model proposed by Lysaker, Lundervold, and Tai (the LLT model) with the following form:

$$\min_{\overline{u}} \frac{\beta_1}{2} \|\overline{u} - \overline{u}_0\|_{L^2}^2 + |\overline{u}|_{BV^2}, \tag{1.6}$$

where $|\overline{u}|_{BV^2} := \int_\Omega |\nabla^2 \overline{u}| \mathrm{d}x$ for the Hessian operator ∇^2. However, these classes of models can blur the edges of the image in the course of restoration. Therefore, it is a natural choice to combine advantages of the ROF model and the LLT model if we want to preserve edges while avoiding the staircase effect in smooth regions. One of convex combinations between the BV and BV^2 was proposed by Lysaker et al. [13] to restore the image with additive noise. But their model is not quite intuitive due to lack of gradient information in the weighting

function. Since the edge detector function $g := g(u_0) := 1/(1 + \varrho|\nabla(u_0 * G_\sigma(x))|)$ with $G_\sigma(x) = (1/2\pi\sigma^2)\exp(-(x^2/2\sigma^2))$ can depict the information of edges, we can employ it as a balance function; that is, we can apply the following model:

$$\min_u \frac{\beta}{2}\|u - \overline{u}_0\|_{L^2}^2 + |(1 - g)u|_{BV} + |gu|_{BV^2} \tag{1.7}$$

to restore the noisy image [16]. Obviously, $|(1 - g)u|_{BV}$ tends to be predominant where edges most likely appear and $|gu|_{BV^2}$ tends to be predominant at the locations with smooth signals. Based on the advantages of the hybrid model (1.7), we also extend it to the image restoration models (1.3)–(1.5) in this paper.

Another topic for image restoration is to find some efficient methods to solve the above proposed models. In fact, there are many different methods based on PDE or convex optimization to solve the minimization problem (1.1) by means of the specific models (1.2)–(1.6). For example, for the purpose of solving the ROF model (1.2) or the LLT model (1.6), we can use the gradient descent method [5, 13], the Chambolle's dual method [13, 17, 18], the primal and dual method [19–21], the second order cone programming method [22], the multigrid method [23], operator splitting method [24–26], the inverse scale method [27], and so forth. However, different from the ROF model (1.2) and the LLT model (1.6), the model (1.7) includes two L^1-norm terms which make it solved more difficultly. More generally, the model (1.7) can be fell into the following framework:

$$\min_u \frac{\theta}{2}\|u - f\|_{L^2}^2 + h_1(\Lambda_1 u) + h_2(\Lambda_2 u), \tag{1.8}$$

where $h_1, h_2 : \mathcal{X} \rightarrow \mathrm{R}$ are proper, convex, and lower semicontinuous (l.s.c.), Λ_1 and Λ_2 are bounded linear operators, and θ is a parameter. A specific form of (1.8) was considered by Afonso and Bioucas-Dias in [28] where a Bregman iterative method was proposed to solve the model with the combination of the L^1-norm term and the total variation (TV) term. Actually this splitting Bregman method is formally equivalent to the alternating direction method of multipliers (ADMM) [24, 29–34]. However, the ADMM ineluctably tends to solve some subproblems which correspond to the related modified problems. Furthermore, these make us obtain the numerical results by requiring much more computational cost. In order to obtain an efficient numerical method, it is a natural choice to avoid solving the related subproblems. In this paper, we propose a proximal point method (PPM) which can be deduced from the ADMM. This deduction is based on the connection that the sum of the projection operator and the shrinkage operator is equal to the identity operator; it is known as the Moreau-Yosida decomposition Theorem 31.5 in [35]. Then the PPM not only keeps the advantages of the ADMM but also requires much less computational cost. This implies that the PPM is much more fast and efficient, especially for the larger scale images. Furthermore, using the monotone operator theory, we give the convergence analysis of the proposed method. Moreover, we extend the PPM to solve the model (1.7) to image deblurring, image inpainting, and the multiplicative noisy image restoration. Experimental results show that the restored images generated by the proposed models and methods are desirable.

The paper is organized as follows. In Section 2, we recall some knowledge related to convex analysis. In Section 3, we first propose the ADMM to solve the problem (1.8) and then give the PPM to improve this method. In Section 4, we give some applications by using the

proposed algorithms and also compare the related models and the proposed methods. Some concluding remarks are given in Section 5.

2. Notations and Definitions

Let us describe some notations and definitions used in this paper. For simplifying, we use $X = R^n$. Usually, we can set $n = 2$ for the gray-scale images. The related contents can be referred to [1, 27, 36–43].

Definition 2.1. The operator $A : X \rightarrow R$ is monotone if it satisfies

$$(y_1 - y_2, x_1 - x_2) \geq 0 \tag{2.1}$$

for all $y_1 \in A(x_1)$ and $y_2 \in A(x_2)$, and A is maximal if it is not strictly contained in any other monotone operator on X.

Definition 2.2. Let $G : X \rightarrow R \cup \{+\infty\}$ be a convex function. The subdifferential of G at a point $y \in X$ is defined by

$$\partial G(y) = \{\eta : G(y) - G(x) \leq (\eta, y - x), \ \forall x \in X\}, \tag{2.2}$$

where $\eta \in \partial G(y)$ is called a subgradient. It reduces to the classical gradient if $G(x)$ is differentiable.

Definition 2.3. Assume that A is a maximal monotone operator. Denote by H_c its Yosida approximation:

$$H_{cA} = \frac{1}{c}(I - J_{cA}), \tag{2.3}$$

where I denotes the identity operator [38, 39] and J_{cA} is the resolvent of A with the form as

$$J_{cA} = (I + cA)^{-1}. \tag{2.4}$$

Definition 2.4. Let $G : X \rightarrow R$ be a convex proper function. The conjugate function of G is defined by

$$G^*(x^*) = \sup_{x \in X}\{(x, x^*) - G(x)\} \tag{2.5}$$

for all $x^* \in X$.

Definition 2.5. Let $G : X \rightarrow R \cup \{\infty\}$ be convex and $t > 0$. The proximal mapping to $G : X \rightarrow X$ is defined by

$$\text{Prox}_t G(x) := \arg \min_y \left\{ G(y) + \frac{1}{2t} \|y - x\|_{L^2}^2 \right\} \tag{2.6}$$

for $y \in X$.

Definition 2.6. The projection operator $\mathcal{P}_{\mathcal{B}_\tau}(\cdot) : X \rightarrow X$ onto the closed disc $\mathcal{B}_\tau := \{x \in X : |x|_{L^1} \leq 1/\tau\}$ is defined by

$$\mathcal{P}_{\mathcal{B}_\tau}(x) = \frac{x}{|x|_{L^1}} \min \left(|x|_{L^1}, \frac{1}{\tau} \right), \tag{2.7}$$

where $x \in X$ and $\tau > 0$.

Definition 2.7. The shrinkage operator $S_\tau(\cdot) : X \rightarrow X$ is defined by

$$S_\tau(x) = \frac{x}{|x|_{L^1}} \max \left(|x|_{L^1} - \frac{1}{\tau}, 0 \right), \tag{2.8}$$

where we use the convention $0/0 = 0$.

Remark 2.8. It is obvious that the function $G : X \rightarrow R$ and its conjugate function G^* satisfy the following relationship:

$$\text{Prox}_t G(x) + \text{Prox}_{1/t} G^*(x) = x, \tag{2.9}$$

for $t > 0$. Especially, the projection operator $\mathcal{P}_{\mathcal{B}_\tau}(\cdot)$ and the shrinkage operator $S_\tau(\cdot)$ satisfy

$$\mathcal{P}_{\mathcal{B}_\tau}(x) + S_\tau(x) = x \tag{2.10}$$

for any $x \in X$. In fact, this corresponds to the classic Moreau-Yosida decomposition Theorem 31.5 in [35].

3. The Alternating Direction Method of Multipliers (ADMM) and the Proximal Point Method (PPM)

Variable splitting methods such as the ADMM [29–32, 44] and the operator splitting methods [42, 45, 46] have been recently used in the image, signal, and data processing community. The key of this class of methods is to transform the original problem into some subproblems so that we can easily solve these subproblems by employing some numerical methods. In this section we first consider to use the ADMM to solve the general minimization problem (1.8). However, the computational cost of the ADMM is tediously increased due to its looser form. In order to overcome this drawback, we thus change this method to a compacter form called the proximal method based on the relationship (2.9) in Remark 2.8.

3.1. The Alternating Direction Method of Multipliers (ADMM)

We now consider the following constrained problem:

$$\min_{u,v,w} \frac{\theta}{2}\|u - f\|_{L^2}^2 + h_1(v) + h_2(z),$$

$$\text{s.t.} \quad v = \Lambda_1 u, \quad z = \Lambda_2 u, \tag{3.1}$$

which is clearly equivalent to the constrained problem (1.8) in the feasible set $\{(u, v, z) : v = \Lambda_1 u, \text{ and } z = \Lambda_2 u\}$. Throughout the following subsections, we always assume that Λ_1 and Λ_2 are a surjective map. It seems that the problem (3.1) including three variables looks more complex than the original unconstrained problem (1.8). In fact, this problem can be solved more easily under the condition that h_1 and h_2 are nondifferentiable. In the augmented Lagrangian framework [33, 34, 47, 48], the problem (3.1) equivalently solves the following minimization Lagrangian function:

$$\min_{u,v,z,\zeta_1,\zeta_2,\mu_1,\mu_2} L(u, v, z, \zeta_1, \zeta_2, \mu_1, \mu_2) = \frac{\theta}{2}\|u - f\|_{L^2}^2 + h_1(v) + (\zeta_1, \Lambda_1 u - v) + \frac{\mu_1}{2}\|\Lambda_1 u - v\|_{L^2}^2$$

$$+ h_2(z) + (\zeta_2, \Lambda_2 u - z) + \frac{\mu_2}{2}\|\Lambda_2 u - z\|_{L^2}^2, \tag{3.2}$$

where ζ_i is the Lagrangian multiplier and μ_i is the penalty parameter for $i = 1, 2$. Then we can use the following augmented Lagrangian method (ALM):

$$(u^n, v^n, z^n) = \arg\min_{u,v,z} L(u, v, z, \zeta_1^{n-1}, \zeta_2^{n-1}, \mu_1, \mu_2), \tag{3.3a}$$

$$\zeta_1^n = \zeta_1^{n-1} + \mu_1(\Lambda_1 u - v), \tag{3.3b}$$

$$\zeta_2^n = \zeta_2^{n-1} + \mu_2(\Lambda_2 u - z) \tag{3.3c}$$

with choosing the original values ζ_1^0 and ζ_2^0 to solve (3.2). If we set $d_i^n = \zeta_i^n/\mu_i$ for $i = 1, 2$ and omit the terms which are independent of (u^n, v^n, z^n) in (3.3a), the above strategy (3.3a)–(3.3c) can be written as

$$(u^n, v^n, z^n) = \arg\min_{u,v,z} \frac{\theta}{2}\|u - f\|_{L^2}^2 + h_1(v) + \frac{\mu_1}{2}\|\Lambda_1 u - v + d_1^{n-1}\|_{L^2}^2 + h_2(z),$$

$$+ \frac{\mu_2}{2}\|\Lambda_2 u - z + d_2^{n-1}\|_{L^2}^2, \tag{3.4a}$$

$$d_1^n = d_1^{n-1} + \Lambda_1 u^n - v^n, \tag{3.4b}$$

$$d_2^n = d_2^{n-1} + \Lambda_2 u^n - z^n \tag{3.4c}$$

for the original values d_1^0 and d_2^0. Then we can use the following ADMM to solve (3.4a)–(3.4c).

Algorithm 3.1 (ADMM for solving (3.4a)–(3.4c)). (1) Choose the original values: v^0, z^0, d_1^0, and d_2^0. Set θ, μ_1, $\mu_2 > 0$ and $n = 1$.

(2) Compute $(u^n, v^n, z^n, d_1^n, d_2^n)$ by

$$u^n = \arg\min_u \underbrace{\frac{\theta}{2}\|u - f\|_{L^2}^2 + \frac{\mu_1}{2}\left\|\Lambda_1 u - v^{n-1} + d_1^{n-1}\right\|_{L^2}^2 + \frac{\mu_2}{2}\left\|\Lambda_2 u - z^{n-1} + d_2^{n-1}\right\|_{L^2}^2}_{=h(u)}, \tag{3.5a}$$

$$v^n = \arg\min_v h_1(v) + \frac{\mu_1}{2}\left\|\Lambda_1 u^n - v + d_1^{n-1}\right\|_{L^2}^2, \tag{3.5b}$$

$$z^n = \arg\min_z h_2(z) + \frac{\mu_2}{2}\left\|\Lambda_2 u^n - z + d_2^{n-1}\right\|_{L^2}^2, \tag{3.5c}$$

$$d_1^n = d_1^{n-1} + \Lambda_1 u^n - v^n, \tag{3.5d}$$

$$d_2^n = d_2^{n-1} + \Lambda_2 u^n - z^n. \tag{3.5e}$$

(3) If the stop criterion is not satisfied, set $n := n + 1$ and go to step (2).

Since $h(u)$ is differentiable and strictly convex, we can get the unique solution of (3.5a) which satisfies

$$\theta(u^n - f) + \mu_1 \Lambda_1^*\left(\Lambda_1 u^n - v^{n-1} + d_1^{n-1}\right) + \mu_2 \Lambda_2^*\left(\Lambda_2 u^n - z^{n-1} + d_2^{n-1}\right) = 0, \tag{3.6a}$$

$$0 = w_1^n + \mu_1\left(v^n - d_1^{n-1} - \Lambda_1 u^n\right), \tag{3.6b}$$

$$0 = w_2^n + \mu_2\left(z^n - d_2^{n-1} - \Lambda_2 u^n\right), \tag{3.6c}$$

$$d_1^n = d_1^{n-1} + \Lambda_1 u^n - v^n, \tag{3.6d}$$

$$d_2^n = d_2^{n-1} + \Lambda_2 u^n - z^n, \tag{3.6e}$$

where Λ_1^* and Λ_2^* are the adjoint operators of Λ_1 and Λ_2, $w_1^n \in \partial h_1(v^n)$ and $w_2^n \in \partial h_2(z^n)$, respectively. It follows that the solution u^n in (3.6a) can be directly obtained by the following explicit formulation:

$$u^n = \underbrace{\left(\theta I + \mu_1 \Lambda_1^* \Lambda_1 + \mu_2 \Lambda_2^* \Lambda_2\right)^{-1}}_{M}\left(\theta f + \mu_1 \Lambda_1^*\left(v^{n-1} - d_1^{n-1}\right) + \mu_2 \Lambda_2^*\left(z^{n-1} - d_2^{n-1}\right)\right). \tag{3.7}$$

However, when the operator M is ill-posed, the solution is unsuitable or unavailable. Hence we have to go back to (3.6a) and to employ some iteration strategy such as the Gauss-Seidel method to solve this equation. On the other hand, it is obvious that (3.5b) and (3.5c) can be

looked at as the proximal mapping, so the solutions of the minimization problems (3.5b) and (3.5c) can be obviously written as

$$v^n = \text{Prox}_{1/\mu_1} h_1\left(\Lambda_1 u^n + d_1^{n-1}\right), \qquad z^n = \text{Prox}_{1/\mu_2} h_2\left(\Lambda_2 u^n + d_2^{n-1}\right). \tag{3.8}$$

Theorem 3.2. *Assume that* $(u^*, v^*, z^*, w_1^*, w_2^*)$ *is the saddle point of the Lagrange function*

$$\mathcal{L}(u, v, z, w_1, w_2) = \frac{\theta}{2}\|u - f\|_{L^2}^2 + h_1(v) + (w_1, \Lambda_1 u - v) + h_2(z) + (w_2, \Lambda_2 u - z). \tag{3.9}$$

Then u^* *is the solution of the minimization problem* (1.8). *Furthermore, the sequence* $\{(u^n, v^n, z^n)\}$ *generated by Algorithm 3.1 converges to* (u^*, v^*, z^*).

Notice that Algorithm 3.1 can be actually looked at as the split Bregman method [25]. The based idea of this method is to introduce some intermediate variables so as to transform the original problem into some subproblems which are easily solved. The connection between the split Bregman method and the ADMM has been shown in [29, 49]. However, our algorithm considers the sum of three convex functions, which is more general than the related algorithms in [25, 49]. Furthermore, it must be noted that v and z are completely separated in (3.4a), so the two subproblems (3.5b) and (3.5c) are parallel. Therefore the convergence results of the ADMM can be applied here.

3.2. The Proximal Point Method

Though the ADMM in Algorithm 3.1 can effectively solve the original problem (3.1), we have to solve five subproblems. This actually makes this method suffer from a looser form as in [25, 45] so that it can badly affect its numerical computation efficiency. In this subsection, we propose a compacter form comparing to the ADMM. This formation called the PPM by using the relationship (2.9) in Remark 2.8 can reduce the original five subproblems of the ADMM in Algorithm 3.1 to solve three subproblems, thus it can improve computation cost of the ADMM. Now we have rewritten (3.5a)–(3.5e) with a little variation as the following form:

$$v^n = \arg\min_v h_1(v) + \frac{\mu_1}{2}\left\|v - d_1^{n-1} - \Lambda_1 u^{n-1}\right\|_{L^2}^2, \tag{3.10a}$$

$$z^n = \arg\min_z h_2(z) + \frac{\mu_2}{2}\left\|z - d_2^{n-1} - \Lambda_2 u^{n-1}\right\|_{L^2}^2, \tag{3.10b}$$

$$d_1^n = d_1^{n-1} + \Lambda_1 u^{n-1} - v^n, \tag{3.10c}$$

$$d_2^n = d_2^{n-1} + \Lambda_2 u^{n-1} - z^n, \tag{3.10d}$$

$$u^n = \arg\min_u \frac{\theta}{2}\|u - f\|_{L^2}^2 + \frac{\mu_1}{2}\left\|\Lambda_1 u - v^n + d_1^n\right\|_{L^2}^2 + \frac{\mu_2}{2}\left\|\Lambda_2 u - z^n + d_2^n\right\|_{L^2}^2 \tag{3.10e}$$

with the first order optimality conditions given by

$$v^n = \text{prox}_{1/\mu_1} h_1\left(\Lambda_1 u^{n-1} + d_1^{n-1}\right), \tag{3.11a}$$

$$z^n = \text{prox}_{1/\mu_1} h_2\left(\Lambda_2 u^{n-1} + d_2^{n-1}\right), \tag{3.11b}$$

$$d_1^n = d_1^{n-1} + \Lambda_1 u^{n-1} - v^n, \tag{3.11c}$$

$$d_2^n = d_2^{n-1} + \Lambda_2 u^{n-1} - z^n, \tag{3.11d}$$

$$\theta(u^n - f) + \mu_1 \Lambda_1^*(\Lambda_1 u^n - v^n + d_1^n) + \mu_2 \Lambda_2^*(\Lambda_2 u^n - z^n + d_2^n) = 0. \tag{3.11e}$$

If (3.11e) is replaced by

$$\theta(u^n - f) + \mu_1 \Lambda_1^*\left(\Lambda_1 u^{n-1} - v^n + d_1^{n-1}\right) + \mu_2 \Lambda_2^*\left(\Lambda_2 u^{n-1} - z^n + d_2^{n-1}\right) = 0, \tag{3.12}$$

it follows from (3.11a)–(3.11e) and Moreau-Yosida decomposition Theorem 31.5 in [35] that

$$d_1^n = \text{prox}_{\mu_1} h_1^*\left(\Lambda_1 u^{n-1} + d_1^{n-1}\right),$$

$$d_2^n = \text{prox}_{\mu_2} h_2^*\left(\Lambda_2 u^{n-1} + d_2^{n-1}\right), \tag{3.13}$$

$$u^n = f - \left(\frac{\mu_1}{\theta}\Lambda_1^* d_1^n + \frac{\mu_2}{\theta}\Lambda_2^* d_2^n\right).$$

So we propose the following algorithm to solve (3.1).

Algorithm 3.3 (PPM for solving (3.1)). (1) Choose the original values: d_1^0, d_2^0, and u^0. Set θ, μ_1, $\mu_2 > 0$ and $n = 1$.
    (2) Compute (d_1^n, d_2^n, u^n) by (3.13).
    (3) If the stop criterion is not satisfied, set $n := n + 1$ and go to step (2).

Lemma 3.4. *Set x_1, $x_2 \in X$ and A is a maximal monotone operator, then the operators H_{cA} and J_{cA} satisfy*

$$\frac{1}{c^2}\|J_{cA}(x_1) - J_{cA}(x_2)\|_{L^2}^2 + \|H_{cA}(x_1) - H_{cA}(x_2)\|_{L^2}^2 \le \frac{1}{c^2}\|x_1 - x_2\|_{L^2}^2. \tag{3.14}$$

Theorem 3.5. *Assume that $h_1(x)$ and $h_2(u)$ are convex and proper. If $\mu_1 \in (0, 1/\theta\|\Lambda_1\|^2)$ and $\mu_2 \in (0, 1/\theta\|\Lambda_2\|^2)$, here $\|\cdot\| := \max\{\|Kx\|_{L^2} : x \in X$ with $\|x\|_{L^2} \le 1\}$ for a continuous linear operator K, then the sequence $\{(u^n, d_1^n, d_2^n)\}$ generated by Algorithm 3.3 converges to the limit point $(\overline{d}_1, \overline{d}_2, \overline{u})$. Furthermore, the limit point $\overline{u}$ is the solution of (1.8).*

4. Some Applications in Image Restoration

In Section 4.1, we apply the ADMM and the above PPM to the image denoising problem. Here we also compare the proposed hybrid model with the ROF model and the LLT model. Then, based on the proposed hybrid model, we set the PPM as a basic method to solve image deblurring, image inpainting, and image denoising for the multiplicative noise in the last three subsections. For simplicity, we assume that the image region Ω is squared with the size $M \times M$ and set $S = R^{M \times M}$, $T = S \times S$, and $Z = T \times T$ as in [17]. The usual scalar product can be denoted as $\langle p^1, p^2 \rangle_T := \sum_{i=1}^{M} \sum_{j=1}^{M} p_{i,j}^1 p_{i,j}^2$ for $p^1, p^2 \in T$ and $(\mathbf{p}, \mathbf{q})_Z = \sum_{i,j=1}^{M} (p_{i,j}^{11} q_{i,j}^{11} + p_{i,j}^{12} q_{i,j}^{12} + p_{i,j}^{21} q_{i,j}^{21} + p_{i,j}^{22} q_{i,j}^{22})$ for $\mathbf{p}, \mathbf{q} \in Z$. The L^1 norm of $\mathbf{p} = (p_1, p_2) \in T$ is defined by $|\mathbf{p}|_{\ell^1} = \sqrt{p_1^2 + p_2^2}$ and the ℓ^1 norm of $\mathbf{q} = (q_1, q_2; q_3, q_4) \in Z$ is defined by $|\mathbf{q}|_{\ell^1} = \sqrt{q_1^2 + q_2^2 + q_3^2 + q_4^2}$. If $u \in S$, we use $\nabla^+ = (\nabla_x^+, \nabla_y^+) \in T$ to denote the first order forward difference operator with

$$\nabla_x^+ u_{i,j} = \begin{cases} u_{i+1,j} - u_{i,j} & \text{for } 1 \leq i < N, \\ 0 & \text{for } i = N, \end{cases} \qquad \nabla_y^+ u_{i,j} = \begin{cases} u_{i,j+1} - u_{i,j} & \text{for } 1 \leq j < N, \\ 0 & \text{for } j = N, \end{cases} \tag{4.1}$$

and use $\nabla^- = (\nabla_x^-, \nabla_y^-)$ to denote the first order backward difference operator with

$$\nabla_x^- u_{i,j} = \begin{cases} -u_{i,j}, & \text{for } i = 1, \\ u_{i,j} - u_{i-1,j} & \text{for } 1 < i < N, \\ u(i,j) & \text{for } i = N, \end{cases} \qquad \nabla_y^- u_{i,j} = \begin{cases} -u_{i,j} & \text{for } j = 1, \\ u_{i,j} - u_{i,j-1} & \text{for } 1 < j < N, \\ u_{i,j} & \text{for } j = N, \end{cases} \tag{4.2}$$

for $i, j = 1, \ldots, N$. Based on the first order difference operators, we can give the second order difference operator as follows:

$$\nabla^2 u_{i,j} = \begin{pmatrix} \nabla_x^-(\nabla_x^+ u_{i,j}) & \nabla_x^+(\nabla_y^+ u_{i,j}) \\ \nabla_y^-(\nabla_x^- u_{i,j}) & \nabla_y^-(\nabla_y^+ u_{i,j}) \end{pmatrix} \in Z. \tag{4.3}$$

Using the same approach, we can define some other second order operators such as $\nabla_x^+(\nabla_x^- u_{i,j})$, $\nabla_x^-(\nabla_y^- u_{i,j})$, $\nabla_y^+(\nabla_x^+ u_{i,j})$, and $\nabla_y^+(\nabla_y^- u_{i,j})$. Then we can give the first order and the second divergence operators as

$$\text{div } u_{i,j} = \nabla_x^- u_{i,j} + \nabla_y^- u_{i,j},$$

$$\text{div}^2 u_{i,j} = \nabla_x^+(\nabla_x^- u_{i,j}) + \nabla_x^-(\nabla_y^- u_{i,j}) + \nabla_y^+(\nabla_x^- u_{i,j}) + \nabla_y^+(\nabla_y^- u_{i,j}). \tag{4.4}$$

Furthermore, if we set $\mathbf{p} \in T$ and $\mathbf{q} \in Z$, it is easy to deduce that

$$\|\text{div } p\|_2^2 \leq 8\|\mathbf{p}\|_T^2, \qquad \|\text{div}^2 q\|_2^2 \leq 64\|\mathbf{q}\|_Z^2. \tag{4.5}$$

Remark 4.1. The related examples in the following subsections are performed using Windows 7 and Matlab 2009(a) on a desktop with Intel Core i5 processor at 2.4 GHz and 4 GB memory. All of the parameters for related models are chosen by trial and empirically which can yield better restored images. On the other hand, we should notice that it is not very expensive when we use the ADMM and the PPM to get u^n, but the total computational effort of one outer iteration requiring many inner steps can be very huge. In order to reduce the computational effort and keep fair comparison of these two methods, we so simplify the inner-outer iterative framework by performing only one-step in inner iteration. It is obvious that these sets are very efficient from the following numerical experiences.

4.1. Image Denoising for the Additive Noise

In this subsection, we consider to use the ADMM and the PPM to solve (1.7) for restoring the additive noisy image. If we set $\Lambda_1 = \nabla$ and $\Lambda_2 = \nabla^2$, then the algorithms are proposed as follows.

Algorithm 4.2 (ADMM to solve (1.7)). (1) Choose the original $d_1^0 = v^0 = \mathbf{0} \in T$ and $d_2^0 = z^0 = \mathbf{0} \in Z$. Set $\theta, \mu_1, \mu_2 > 0$ and $n = 1$.
    (2) Compute $(u^n, v^n, z^n, d_1^n, d_2^n)$ by

$$\left(\theta I - \mu_1 \Delta + \mu_2 \Delta^2\right) u^n = \theta f + \mu_1 \operatorname{div}\left(v^{n-1} - d_1^{n-1}\right) - \mu_2 \operatorname{div}^2\left(z^{n-1} - d_2^{n-1}\right) \tag{4.6a}$$

$$v^n = \frac{\nabla u^n + d_1^{n-1}}{\left|\nabla u^n + d_1^{n-1}\right|_{\ell^1}} \cdot \max\left(\left|\nabla u^n + d_1^{n-1}\right|_{\ell^1} - \frac{(1 - g(x))}{\mu_1}, 0\right), \tag{4.6b}$$

$$z^n = \frac{\nabla^2 u^n + d_2^{n-1}}{\left|\nabla^2 u^n + d_2^{n-1}\right|_{\ell^1}} \cdot \max\left(\left|\nabla^2 u^n + d_2^{n-1}\right|_{\ell^1} - \frac{g(x)}{\mu_2}, 0\right), \tag{4.6c}$$

$$d_1^n = d_1^{n-1} + \nabla u^n - v^n, \tag{4.6d}$$

$$d_2^n = d_2^{n-1} + \nabla^2 u^n - z^n, \tag{4.6e}$$

where $\Delta = \operatorname{div} \circ \nabla$ and $\Delta^2 = \operatorname{div}^2 \circ \nabla^2$.
    (3) If the stop criterion is not satisfied, set $n := n + 1$ and go to step (2).

Remark 4.3. For the first subproblem (4.6a), we can use the Gauss-Seidel method as shown in [25] to get the solution. However, in this paper, we use the following strategy:

$$u_{i,j}^n = \frac{\theta f_{i,j} + \mu_1 \operatorname{div}\left(v_{i,j}^{n-1} - d_{1,i,j}^{n-1}\right) + 4\mu_1 u_{i,j}^{n-1} - \mu_2 \operatorname{div}^2\left(z_{i,j}^{n-1} - d_{2,i,j}^{n-1}\right) + 28\mu_2 u_{i,j}^{n-1}}{\theta + 4\mu_1 + 28\mu_2}, \tag{4.7}$$

where some information of operators Δ and Δ^2 related to u is used. The formulas (4.6b) and (4.6c) of Algorithm 4.2 can be easily deduced from

$$
\min_v \left| (1 - g)v \right|_{\ell^1} + \frac{\mu_1}{2} \left\| v - \nabla u^n - d_1^{n-1} \right\|_2^2,
$$
$$
\min_z \left| gv \right|_{\ell^1} + \frac{\mu_2}{2} \left\| z - \nabla^2 u^n - d_2^{n-1} \right\|_2^2.
\tag{4.8}
$$

Furthermore, following form Theorem 3.2, we can also deduce that the sequence $\{u^n\}$ generated by Algorithm 4.2 converges to the solution of (1.7).

Algorithm 4.4 (PPM to solve (1.7)). (1) Choose the original $d_1^0 = 0 \in S$, $d_2^0 = 0 \in Z$ and $u^0 = f$. Set $\theta, \mu_1, \mu_2 > 0$ and $n = 1$.
 (2) Compute (d_1^n, d_2^n, u^n) by

$$
d_1^n = \frac{\nabla u^{n-1} + d_1^{n-1}}{\left| \nabla u^{n-1} + d_1^{n-1} \right|_{\ell^1}} \cdot \min\left(\left| \nabla u^{n-1} + d_1^{n-1} \right|_{\ell^1}, 1 \right),
$$
$$
d_2^n = \frac{\nabla^2 u^{n-1} + d_2^{n-1}}{\left| \nabla^2 u^{n-1} + d_2^{n-1} \right|_{\ell^1}} \cdot \min\left(\left| \nabla^2 u^{n-1} + d_2^{n-1} \right|_{\ell^1}, 1 \right),
\tag{4.9}
$$
$$
u^n = f - \frac{\mu_1}{\theta}(1 - g)\operatorname{div} d_1^n + \frac{\mu_2}{\theta} g\operatorname{div}^2 d_2^n.
$$

(3) If the stop criterion is not satisfied, set $n := n + 1$ and go to step (2).

For Algorithm 4.4, based on the relations in (4.5) and Theorem 3.5, we have the following result.

Theorem 4.5. *If $\mu_1 \in (0, 1/8\theta)$ and $\mu_2 \in (0, 1/64\theta)$, then the sequence $\{u^n\}$ generated by Algorithm 4.4 converges to the solution of (1.7).*

Remark 4.6. For the above two algorithms, we can also set g as a constant between 0 and 1. In fact, it is easy to find that the algorithms correspond to solving the ROF model or the LLT model, respectively, when $g = 0$ or $g = 1$. At this time, the iteration strategy can be simplified as

$$
u_{i,j}^n = \frac{\theta f_{i,j} + \mu_1 \operatorname{div}\left(v_{i,j}^{n-1} - d_{1,i,j}^{n-1} \right) + 4\mu_1 u_{i,j}^{n-1}}{\theta + 4\mu_1},
$$
$$
u_{i,j}^n = \frac{\theta f_{i,j} - \mu_2 \operatorname{div}^2\left(z_{i,j}^{n-1} - d_{2,i,j}^{n-1} \right) + 28\mu_2 u_{i,j}^{n-1}}{\theta + 28\mu_2}
\tag{4.10}
$$

for these two models, respectively. Furthermore, when $g \in (0, 1)$, these two algorithms correspond to solve the model which is the convex combination of the ROF model and the LLT model.
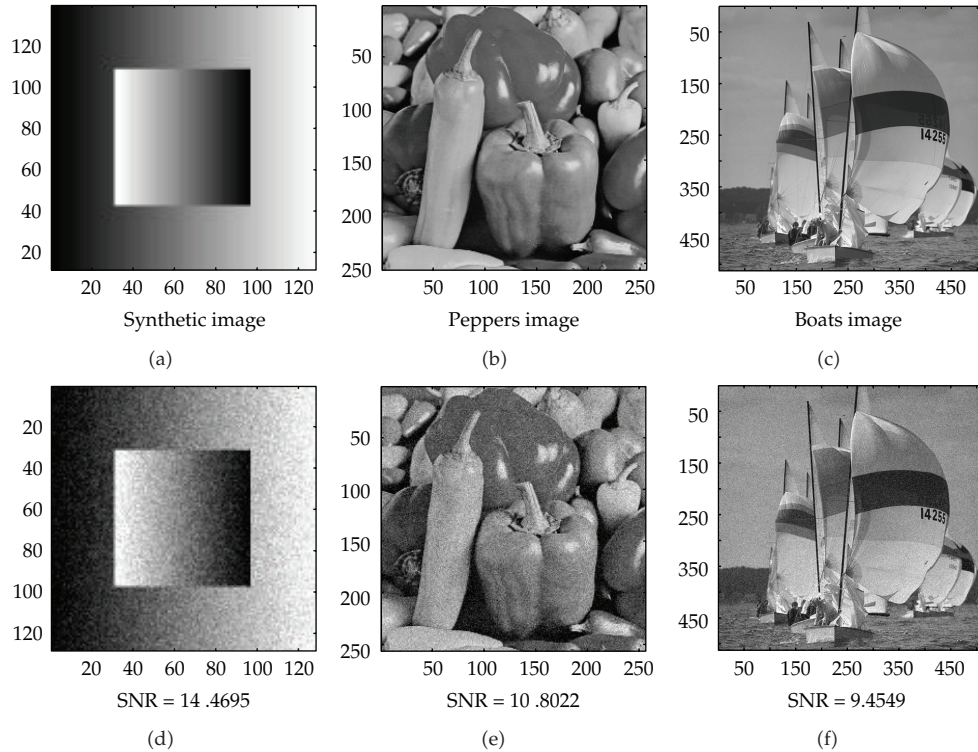
Synthetic image

(a)

Peppers image

(b)

Boats image

(c)

SNR = 14 .4695

(d)

SNR = 10 .8022

(e)

SNR = 9.4549

(f)

Figure 1: The original images and the noisy images with three different sizes in Example 4.7.

Example 4.7. In this example, we compare the ADMM with the PPM for solving the ROF model (1.4), the LLT model (1.6), and the hybrid model (1.7). The original images with three different sizes shown in Figure 1 are added to the Gaussian white noise with the standard deviation $\sigma = 15.3$. Iterations were terminated when the stop conditions $\|u^{n+1} - u^n\|_2 / \|u^n\|_2 \leq \varepsilon$ are met. It is easy to find the related results from Table 1 that the PPM is faster than the ADMM. Especially, the average CPU time of the PPM compared with that of the ADMM can save about 50% for the ROF model and the LLT model. It saves about 40% for the hybrid model.

Example 4.8. In this example, the noisy image is added to the Gaussian white noisy with the standard deviation $\sigma = 12$. The algorithms will be stopped after 100 iterations. We compare the results generated by the ROF model, the LLT model, the convex combination of the ROF model and the hybrid model. As we can see from Table 2, the hybrid model get the lowest MSE and the highest SNR; these imply that the hybrid model can give the best restored image. On the other hand, it is easy to find that the ROF model makes staircasing effect appear and the LLT model leads to edge blurring. In fact, they are based on the fact that the restored model by the ROF model is piecewise constant on large areas and the LLT model as a higher model damps oscillations much faster in the region of edges. For the convex combined model and the hybrid model, they can efficiently suppress these two drawbacks. Furthermore, the hybrid model is more efficient than the convex combined model, because the hybrid model uses the edge detector function which can efficiently coordinate edge information. It should be noticed that here we use the Chambolle's strategy [17] to solve the convex combined

Table 1: The related results in Example 4.7.

$g = 0$		The ROF model					
	Stopping		ADMM			PPM	
Size	Conditions ε	Time (s)	Ite.	SNR	Time (s)	Ite.	SNR
128×128	1.0×10^{-4}	0.2184	86	24.7949	0.1248	83	24.7043
256×256	1.0×10^{-4}	0.9204	77	16.2934	0.2652	38	16.3540
512×512	1.0×10^{-4}	4.3368	64	15.7146	1.9656	53	15.9353
$g = 1$		The LLT model					
	Stopping		ADMM			PPM	
Size	Conditions ε	Time (s)	Ite.	SNR	Time (s)	Ite.	SNR
128×128	1.0×10^{-4}	0.4368	60	24.5688	0.3432	80	25.0287
256×256	1.0×10^{-4}	1.7004	55	16.9065	0.9360	53	16.9083
512×512	1.0×10^{-4}	15.4441	55	15.9432	7.2384	50	15.9512
$g \in (0, 1)$		The hybrid model					
	Stopping		ADMM			PPM	
Size	Conditions ε	Time (s)	Ite.	SNR	Time (s)	Ite.	SNR
128×128	1.0×10^{-4}	0.7176	69	25.7224	0.5304	70	25.4982
256×256	1.0×10^{-4}	2.5584	55	16.9699	1.4664	52	16.9701
512×512	1.0×10^{-4}	19.6561	56	15.9503	9.3445	50	15.9512

Table 2: The related data in Example 4.8 (here R.P. is the regularization parameter).

Model	R.P.	Time (s)	SNR	MSE
ROF	4.5	0.8268	17.7677	44.0400
LLT	3.0	2.0904	17.9998	42.7826
Convex	3.5	2.6832	18.2399	39.7756
Hybrid	4.5	2.5272	18.3694	39.1447

model so that it is slower than the strategy by using the PPM to solve the hybrid model. To focus on these facts, we present some zoomed-in local results and select a slice of the images which meets contours and the smooth regions shown in Figures 2 and 3.

4.2. Other Applications

In this subsection, we extend the hybrid model to other classes of restoration problems. As we can see in Section 4.1, the hybrid model has some advantages compared with the ROF model and the LLT model. Since the PPM is faster and more efficient than the ADMM, we only employ the PPM to solve the related image restoration model. Now we first consider the following iteration strategy:

$$z^n = \mathcal{F}(u^n) =: \arg \min_z \frac{\beta}{2} \|u^n - z\|_{L^2}^2 + h(z), \tag{4.11a}$$

$$u^{n+1} = \mathcal{G}(z^n) := \arg \min_u \frac{\beta}{2} \|u - z^n\|_{L^2}^2 + \underbrace{\int_\Omega |(1 - g)\nabla u| \mathrm{d}x + \int_\Omega |g\nabla^2 u| \mathrm{d}x}_{\mathfrak{D}(u)}, \tag{4.11b}$$
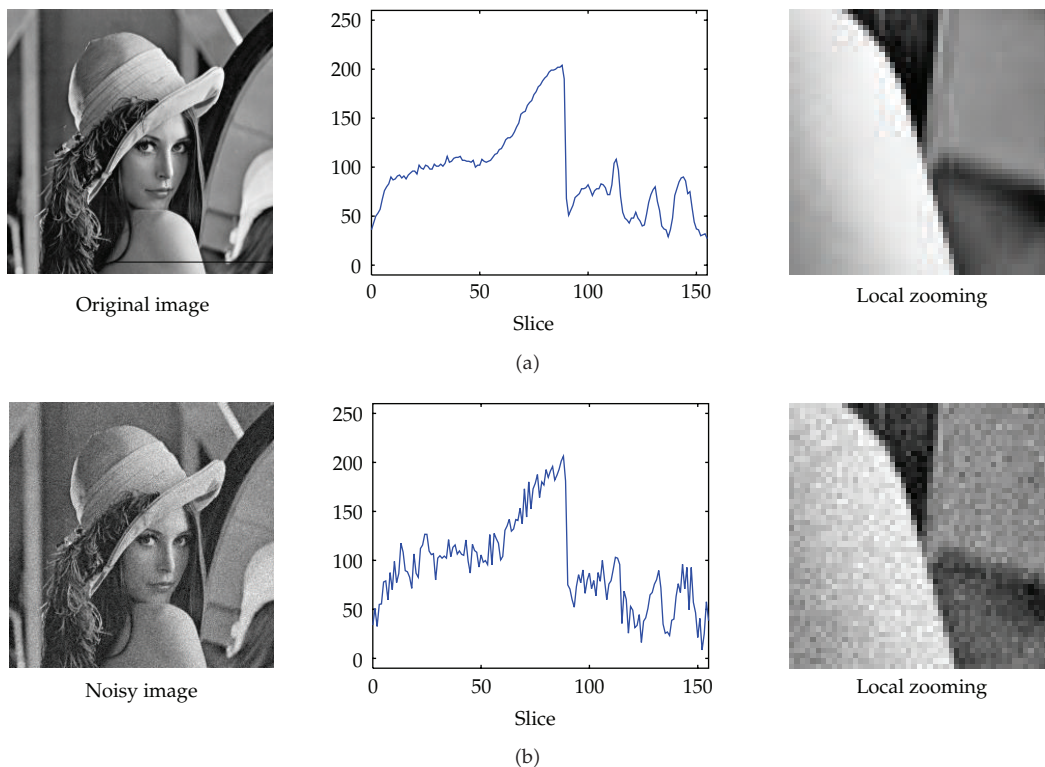
Figure 2: The original and the noisy image in Example 4.8.

where $h(z) \in C^1(\Omega)$. It is easy to find that the minimization problem $\mathfrak{D}(u)$ in (4.11b) is coercive and strictly convex, so the subproblem (4.11b) has a unique solution. Based on [50, Lemma 2.4], we also deduce that the operator $\mathcal{G}$ is $(1/2)$-averaged nonexpansive.

Theorem 4.9. *Assume that the functional*

$$\mathcal{M}(u,z) = \frac{\beta}{2}\|u - z\|_{L^2}^2 + h(z) + \int_{\Omega} |(1 - g)\nabla u|\mathrm{d}x + \int_{\Omega} |g\nabla^2 u|\mathrm{d}x \qquad (4.12)$$

is convex, coercive, and bounded below, then the sequence $\{(u^n, z^n)\}$ generated by (4.11a)-(4.11b) converges to a point (u^*, z^*). Furthermore, when $u^* = z^*$, u^* is the solution of

$$\min_u h(u) + \int_{\Omega} |(1 - g)\nabla u|\mathrm{d}x + \int_{\Omega} |g\nabla^2 u|\mathrm{d}x. \qquad (4.13)$$

Remark 4.10. It should be noticed that the following three models satisfy the conditions of Theorem 4.9, so we can use the strategy (4.11a)-(4.11b) to solve these models.
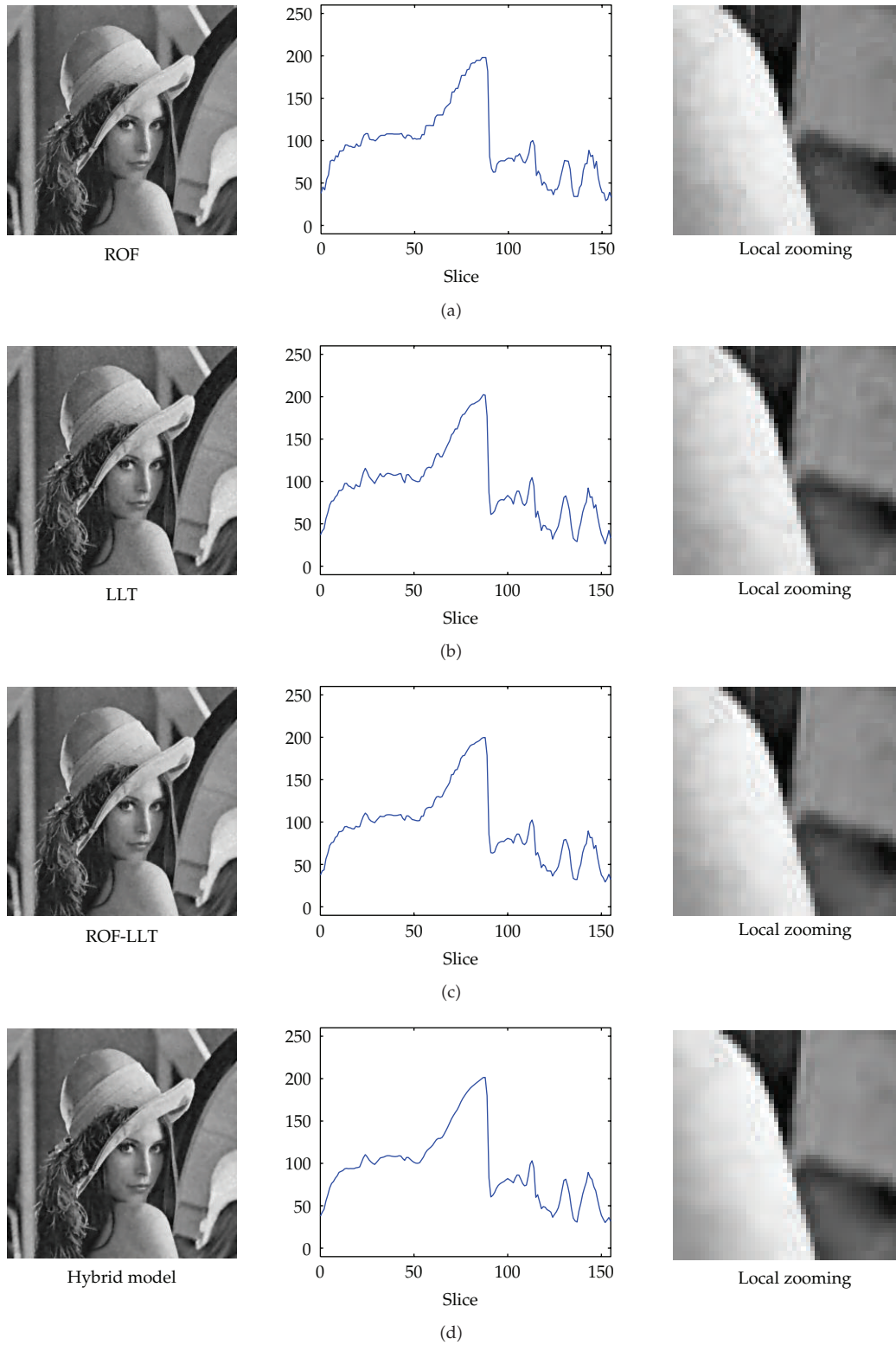
ROF

Local zooming

(a)

LLT

Local zooming

(b)

ROF-LLT

Local zooming

(c)

Hybrid model

Local zooming

(d)

Figure 3: The related restored images in Example 4.8.

4.2.1. Image Deblurring

Now we apply the hybrid model to the image deblurring problems with the following formula:

$$\min_u \frac{\lambda}{2} \|Ku - u_0\|_{L^2}^2 + |u|_{BV_{(1-g)}} + |u|_{BV_g^2}. \tag{4.14}$$

Because of the compactness, the blurring operator K is not continuously invertible, which implies that we cannot directly use the proximal method to solve minimization problem (4.14). However, based on the penalty method [48], we can transform the problem (4.14) to solve the following problem:

$$z^n = \left(\mu\lambda K^T K + I\right)^{-1} \left(\mu\lambda K^T f + u^n\right), \tag{4.15a}$$

$$u^{n+1} := \arg\min_u \frac{1}{2\mu} \|u - z^n\|_{L^2}^2 + \int_\Omega |(1-g)\nabla u| dx + \int_\Omega |g\nabla^2 u| dx. \tag{4.15b}$$

The key of (4.15a)-(4.15b) is to separate the blurring operator K from the original problem (4.14) so that we can avoid the ill-posed operator K. Furthermore, it is obvious that the problem (4.15b) satisfies Theorem 4.9, so we can use the proximal method to solve it.

Example 4.11. In this experiment, we use the image Lena, which is blurred with a Gaussian kernel of "hsize = 3" and in which is added the Gaussian white noise with the standard deviation $\sigma = 0.02$. The related images and SNRs are arranged in Figure 4. As we can see in Example 4.7, the proximal method tends to be stable before 100 iterations, so here we fix the algorithm to be stopped when the iteration attains 100. It is easy to find that the hybrid model can give a better image quality than the other two models. Especially, we also observe some staircasing effect in Figure 4(b) and edge blurring in Figure 4(c). However, all of the drawbacks can be efficiently suppressed in Figure 1(d).

4.2.2. Image Inpainting

Here we consider to use the hybrid model for the image inpainting problem with the following form:

$$\min_u \frac{\overline{\lambda}}{2} \|u - u_0\|_{L^2(\Omega \setminus D)}^2 + |(1-g)u|_{BV} + |gu|_{BV^2}, \tag{4.16}$$

where D is the inpainting domain and $\overline{\lambda}$ satisfies

$$\overline{\lambda} = \begin{cases} \lambda, & \text{if } u \in \Omega \setminus D, \\ 0, & \text{if } u \in D. \end{cases} \tag{4.17}$$

(a) Original image

(b) ROF model

(c) LLT model

(d) Hybrid model

Figure 4: The related SNRs in Example 4.11. (a) 11.2166; (b) 14.3378; (c) 14.4778; (d) 14.5118.

If we introduce an auxiliary variable z, based on the penalty method [48] again, then the solution of the problem (4.15a)-(4.15b) can be approximated by solving the following problem:

$$u^n := \frac{z^n + \overline{\lambda}\mu u_0}{1 + \overline{\lambda}\mu}, \tag{4.18a}$$

$$z^{n+1} := \arg\min_z \frac{1}{2\mu}\|z - u^n\|_{L^2}^2 + \int_\Omega |(1-g)\nabla z|\,\mathrm{d}x + \int_\Omega \left|g\nabla^2 z\right|\,\mathrm{d}x. \tag{4.18b}$$

Example 4.12. In this example, we show the results of real image inpainting in Figures 6 and 7. We consider to use these three models to restore images shown in Figures 5(c) and 5(d), which are, respectively, contaminated by the mask image and the noise with the standard deviation $\sigma = 12$. The parameters of these three models are chosen for getting better restored images and the algorithms will be stopped after 500 iterations (see also Table 3). It is obvious that these three models can efficiently restore the original deteriorated images. However, there are much more inappropriate information restored by the ROF model than the LLT model and the hybrid model. These advantages is based on the fact that the fourth-order

(a) Original image

(b) Mask image

(c) Painting image

(d) Noisy image

Figure 5: The related images in Example 4.12.

Table 3: The related results in Example 4.12.

Model	Image (c) in Figure 5			Image (d) in Figure 5		
	λ	μ	SNR	λ	μ	SNR
ROF	220	0.005	18.5533	32	0.008	15.4055
LLT	150	0.005	16.2934	60	0.005	16.4336
Hybrid	220	0.005	20.2713	70	0.0025	16.6034

linear diffusion (the LLT model and the hybrid model) damps oscillations much faster than second-order diffusion (the ROF model). Especially, these unsuitable effects can be easily seen from the local zooming images in Figures 6 and 7. Furthermore, the restored image by the hybrid model looks more natural than the LLT model.

4.2.3. Image Denoising for the Multiplicative Noise

Based on the hybrid model (1.7), the multiplicative noise model (1.5) can be naturally extended to the following minimization:

$$\min_{z} \alpha \int_{\Omega} (z + f e^{-z}) dx + \int_{\Omega} |(1 - g) \nabla z| dx + \int_{\Omega} |g \nabla^2 z| dx. \qquad (4.19)$$

(a) ROF model   (b) LLT model   (c) Hybrid model

(a1) Local zooming   (b1) Local zooming   (c1) Local zooming
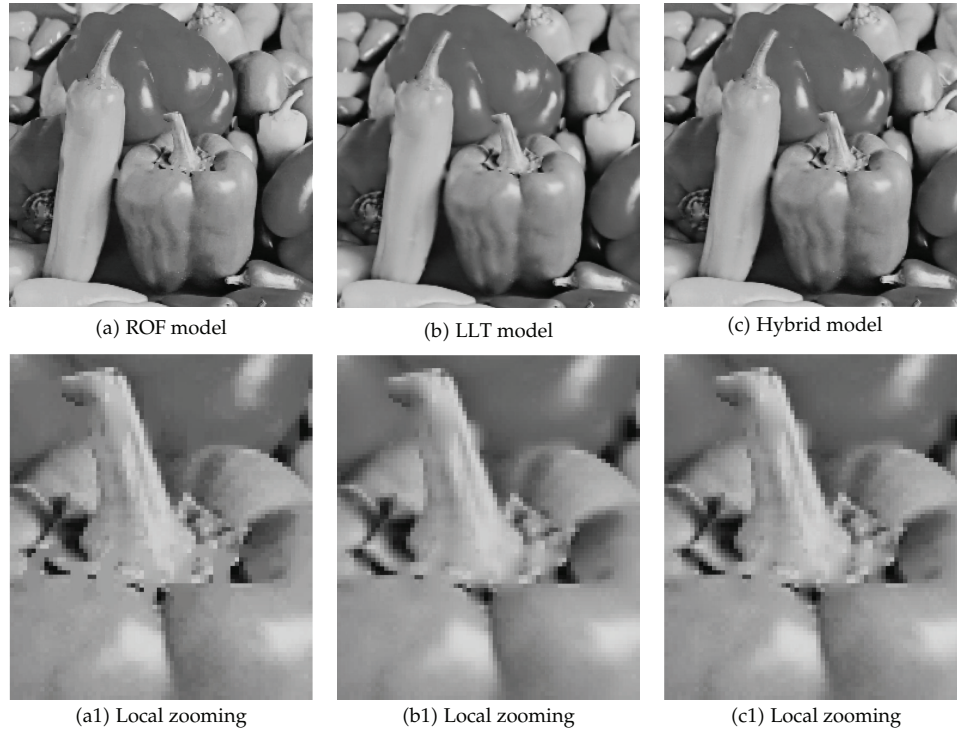
Figure 6: The related restored images corresponding to the painting image in Example 4.12.

It is obvious that the problem (4.19) can be approximated by

$$u^n := \arg \min_u \frac{1}{2\mu} \|z^n - u\|_{L^2}^2 + \alpha \int_\Omega (u + f e^{-u}) \mathrm{d}x, \tag{4.20a}$$

$$z^{n+1} := \arg \min_z \frac{1}{2\mu} \|z - u^n\|_{L^2}^2 + \int_\Omega |(1 - g)\nabla z| \mathrm{d}x + \int_\Omega |g\nabla^2 z| \mathrm{d}x. \tag{4.20b}$$

For the first subproblem (4.20a), its solution u^n can be approximately obtained by using the Newton method to solve the following nonlinear equation:

$$\mu(u - z^n) + \alpha(1 - f e^{-u}) = 0. \tag{4.21}$$

Example 4.13. In this example, we restore the multiplicative noisy image. The noisy Lena image shown in Figure 7 is contaminated by the Gamma noise ($L = 33$) with mean one, in which probability density function $p(u)$ is given by

$$p(u) = \begin{cases} \dfrac{L^L u^{L-1}}{\Gamma(L)} e^{-Lu}, & \text{if } u > 0, \\ 0, & \text{if } u \le 0, \end{cases} \tag{4.22}$$

(a) ROF model   (b) LLT model   (c) Hybrid model

(a1) Local zooming   (b1) Local zooming   (c1) Local zooming
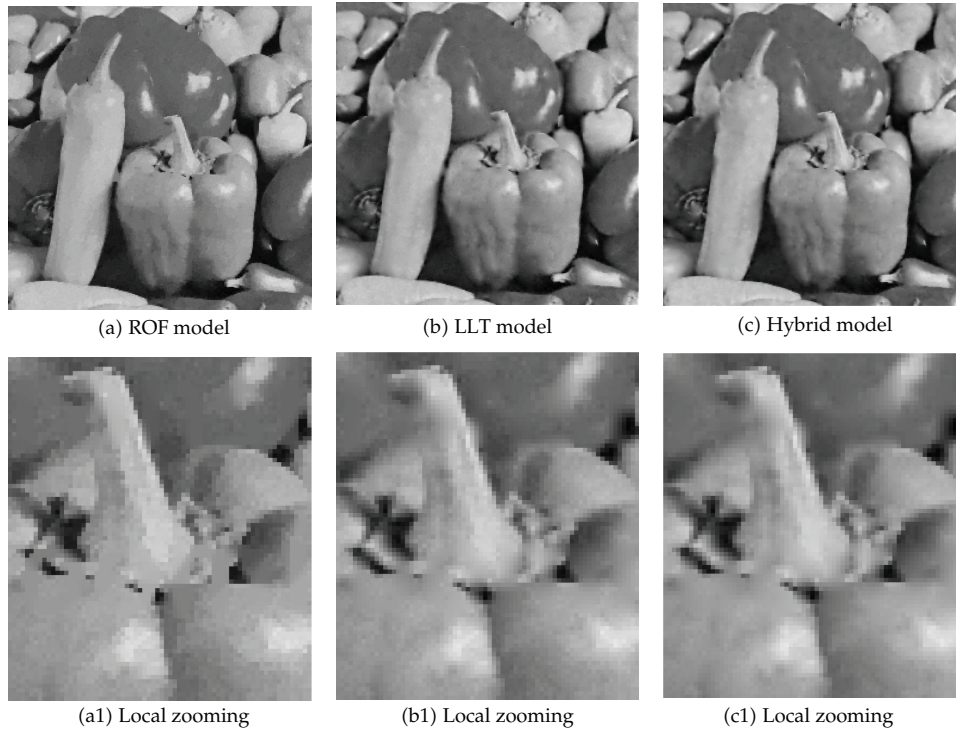
Figure 7: The related restored images corresponding to the noisy image in Example 4.12.

where L is an integer and $\Gamma(\cdot)$ is a Gamma function. Based on the iteration formula (4.20a)-(4.20b), we should notice that there are two interior iterations. For employing the Newton method to solve the problem (4.21), we set the stepsize $t = 1$ and the Newton method will be stopped when $\|u^{n+1} - u^n\|_{\ell^2} / \|u^n\|_{\ell^2} \leq 1.0 \times 10^{-5}$. For solving the second subproblem (4.20b), we set the fixed iterations with 40. In fact for using the PPM to solve the ROF model, the LLT model and the hybrid model, the solutions of these models will tend to the steady. The outer iteration will be stopped after 200 iterations. The related restored images are shown in Figure 8, and it is easy to find that the hybrid model gives a better restored image than the two other models.

5. Concluding Remarks

In this paper, based on the edge detector function, we proposed a hybrid model to overcome some drawbacks of the ROF model and the LLT model. Following the augmented Lagrangian method, we can employ the ADMM of multipliers to solve this hybrid model. In this paper, we mainly proposed the PPM to solve this model due to the fact that the PPM unnecessarily solves a PDE compared with the ADMM so that it is more effective than the ADMM. The convergence of the proposed method was also given. However, the convergence rate of the proposed method is only $O(1/k)$, so our future work is to improve our method with convergence rate $O(1/k^2)$ based on the same strategies in [51, 52].

Appendices

A. Proof of Theorem 3.2

Proof. Following the assumption, we can find that the saddle point $(u^*, v^*, z^*, w_1^*, w_2^*)$ of (3.9) satisfies

$$
\begin{aligned}
0 &= \theta(u^* - f) + \Lambda_1^* w_1^* + \Lambda_2^* w_2^*, \\
0 &= p_1^* - w_1^*, \\
0 &= p_2^* - w_2^*, \\
0 &= \Lambda_1 u^* - v^*, \\
0 &= \Lambda_2 u^* - z^*
\end{aligned}
\tag{A.1}
$$

with $p_1^* \in \partial h_1(v^*)$ and $p_2^* \in \partial h_2(z^*)$. If we set $d_1^* = w_1^*/\mu_1$ and $d_2^* = w_2^*/\mu_2$, then (A.1) can be written as

$$
0 = \theta(u^* - f) + \mu_1 \Lambda_1^* (\Lambda_1 u^* - v^* + d_1^*) + \mu_2 \Lambda_2^* (\Lambda_2 u^* - z^* + d_2^*),
\tag{A.2a}
$$

$$
0 = w_1^* + \mu_1 (v^* - d_1^* - \Lambda_1 u^*),
\tag{A.2b}
$$

$$
0 = w_2^* + \mu_2 (z^* - d_2^* - \Lambda_2 u^*),
\tag{A.2c}
$$

$$
d_1^* = d_1^* + \Lambda_1 u^* - v^*,
\tag{A.2d}
$$

$$
d_2^* = d_2^* + \Lambda_2 u^* - z^*.
\tag{A.2e}
$$

Then the above equations (A.2a)–(A.2e) can be rewritten as a compact form

$$
0 = \theta(u^* - f) + \Lambda_1^* \partial h_1(\Lambda_1 u^*) + \Lambda_2^* \partial h_2(\Lambda_2 u^*),
\tag{A.3}
$$

which implies that u^* is the solution of the minimization problem (1.8).

Set

$$
u_e^n = u^n - u^*, \quad v_e^n = v^n - v^*, \quad z_e^n = z^n - z^*, \quad d_{1e}^n = d_1^n - d_1^*, \quad d_{2e}^n = d_2^n - d_2^*
\tag{A.4}
$$

denote the related errors. Then subtracting (3.6a)–(3.6e) by (A.2a)–(A.2e) and using the similar strategy as in [24], we successively obtain

$$0 = \theta\|u_e^n\|_{L^2}^2 + \mu_1\|\Lambda_1 u_e^n\|_{L^2}^2 + \mu_2\|\Lambda_2 u_e^n\|_{L^2}^2 - \mu_1\left(v_e^{n-1} - d_{1e}^{n-1}, \Lambda_1 u_e^n\right) - \mu_2\left(z_e^{n-1} - d_{2e}^{n-1}, \Lambda_2 u_e^n\right),$$

$$0 = \mu_1\|v_e^n\|_{L^2}^2 + \mu_1\left(v_e^n, d_{1e}^n - d_{1e}^{n-1} - \Lambda_1 u_e^n\right),$$

$$0 = \mu_2\|z_e^n\|_{L^2}^2 + \mu_2\left(z_e^n, d_{2e}^n - d_{2e}^{n-1} - \Lambda_2 u_e^n\right),$$

$$0 = \mu_1\left\|d_{1e}^n\right\|_{L^2}^2 - \mu_1\left\|d_{1e}^{n-1}\right\|_{L^2}^2 + 2\mu_1\left(d_{1e}^{n-1}, v_e^n - \Lambda_1 u_e^n\right) - \mu_1\|v_e^n - \Lambda_1 u_e^n\|_{L^2}^2,$$

$$0 = \mu_2\left\|d_{2e}^n\right\|_{L^2}^2 - \mu_2\left\|d_{2e}^{n-1}\right\|_{L^2}^2 + 2\mu_2\left(d_{2e}^{n-1}, z_e^n - \Lambda_2 u_e^n\right) - \mu_2\|z_e^n - \Lambda_2 u_e^n\|_{L^2}^2,$$

$$\tag{A.5}$$

where $d_{1e}^n \in (1/\mu_1)\partial h_1(v_{1e}^n)$ and $d_{2e}^n \in (1/\mu_2)\partial h_2(z_{1e}^n)$. Summing the above five equations, we get

$$\frac{\mu_1}{2}\left(\left\|d_{1e}^{n-1}\right\|_{L^2}^2 - \|d_{1e}^n\|_{L^2}^2\right) + \frac{\mu_2}{2}\left(\left\|d_{2e}^{n-1}\right\|_{L^2}^2 - \|d_{2e}^n\|_{L^2}^2\right)$$

$$= \theta\|u_e^n\|_{L^2}^2 + \mu_1\left[(d_{1e}^n, v_e^n) + \frac{1}{2}\left\|\Lambda_1 u_e^n - v_e^{n-1}\right\|_{L^2}^2 + \frac{1}{2}\|v_e^n\|_{L^2}^2 - \frac{1}{2}\left\|v_e^{n-1}\right\|_{L^2}^2\right] \tag{A.6}$$

$$+ \mu_2\left[(d_{2e}^n, z_e^n) + \frac{1}{2}\left\|\Lambda_2 u_e^n - z_e^{n-1}\right\|_{L^2}^2 + \frac{1}{2}\|z_e^n\|_{L^2}^2 - \frac{1}{2}\left\|z_e^{n-1}\right\|_{L^2}^2\right].$$

So it is easy to deduce that

$$\frac{\mu_1}{2}\left[\left(\left\|d_{1e}^1\right\|_{L^2}^2 - \left\|d_{1e}^N\right\|_{L^2}^2\right) + \frac{\mu_2}{2}\left(\left\|d_{2e}^1\right\|_{L^2}^2 - \left\|d_{2e}^N\right\|_{L^2}^2\right)\right]$$

$$= \sum_{n=1}^N\left[\theta\|u_e^n\|_{L^2}^2 + \mu_1(d_{1e}^n, v_e^n) + \frac{\mu_1}{2}\left\|\Lambda_1 u_e^n - v_e^{n-1}\right\|_{L^2}^2 + \mu_2(d_{2e}^n, z_e^n) + \frac{\mu_2}{2}\left\|\Lambda_2 u_e^n - z_e^{n-1}\right\|_{L^2}^2\right] \tag{A.7}$$

$$+ \frac{\mu_1}{2}\left\|v_e^N\right\|_{L^2}^2 - \frac{\mu_1}{2}\left\|v_e^1\right\|_{L^2}^2 + \frac{\mu_2}{2}\left\|z_e^N\right\|_{L^2}^2 - \frac{\mu_2}{2}\left\|z_e^1\right\|_{L^2}^2.$$

Following the fact that $h(x)$ is strictly convex, $d_{1e}^n \in (1/\mu)\partial h_1(v_e^n)$ and $d_{2e}^n \in (1/\mu)\partial h_2(z_e^n)$, we can get

$$(d_{1e}^n, v_e^n) \geq 0, \qquad (d_{2e}^n, z_e^n) \geq 0. \tag{A.8}$$

Combined with (A.7), it follows that

$$\sum_{n=1}^N\|u_e^n\|_{L^2}^2 < \infty, \qquad \sum_{n=1}^N\left\|\Lambda_1 u_e^n - v_e^{n-1}\right\|_{L^2}^2 < \infty, \qquad \sum_{n=1}^N\left\|\Lambda_2 u_e^n - z_e^{n-1}\right\|_{L^2}^2 < \infty. \tag{A.9}$$

Then we deduce that

$$\lim_{n \to \infty} u^n = u^*,$$

$$\lim_{n \to \infty} \left\| \Lambda_1 u_e^n - v_e^{n-1} \right\|_{L^2}^2 = 0, \qquad \lim_{n \to \infty} \left\| \Lambda_2 u_e^n - z_e^{n-1} \right\|_{L^2}^2 = 0.$$

(A.10)

So we have

$$\lim_{n \to \infty} \|v^n - v^*\|_{L^2}^2 = 0, \qquad \lim_{n \to \infty} \|z^n - z^*\|_{L^2}^2 = 0.$$

(A.11)

Hence the proof is complete. □

B. Proof of Lemma 3.4

Proof. Let x_i $(i = 1, 2)$ be solutions of

$$x_i \in y_i + cA(y_i),$$

(B.1)

then we can obtain

$$
\begin{aligned}
\|x_1 - x_2\|_{L^2}^2 &= \|y_1 - y_2 + c(A(y_1) - A(y_2))\|_{L^2}^2 \\
&= \|y_1 - y_2\|_{L^2}^2 + c^2 \|A(y_1) - A(y_2)\|_{L^2}^2 + 2c(y_1 - y_2, A(y_1) - A(y_2)) \\
&\geq \|y_1 - y_2\|_{L^2}^2 + c^2 \|A(y_1) - A(y_2)\|_{L^2}^2 \\
&= \|J_{cA} x_1 - J_{cA} x_2\|_{L^2}^2 + c^2 \|H_{cA}(x_1) - H_{cA}(x_2)\|_{L^2}^2,
\end{aligned}
$$

(B.2)

which implies that the assertion holds. □

C. Proof of Theorem 3.5

Proof. Setting $A_1(x) := \partial h_1(x)$ and $A_2(x) := \partial h_2(x)$, then operators A_1 and A_2 are maximal monotone. Following from (3.11a)–(3.11e) and the definition of the Yosida approximation, (3.13) can be equivalently written as

$$\mu_1 d_1^n = H_{A_1/\mu_1}\left(\Lambda_1 u^{n-1} + d_1^{n-1}\right),$$

(C.1a)

$$\mu_2 d_2^n = H_{A_2/\mu_2}\left(\Lambda_2 u^{n-1} + d_2^{n-1}\right),$$

(C.1b)

$$u^n = f - \left(\frac{\mu_1}{\theta}\Lambda_1^* d_1^n + \frac{\mu_2}{\theta}\Lambda_2^* d_2^n\right).$$

(C.1c)

(a) The noisy image

(b) ROF model

(c) LLT model

(d) Hybrid model

(b1) ROF model

(c1) LLT model

(d1) Hybrid model

Figure 8: The related images and the local zooming images in Example 4.13. SNRs: (a) 9.2017; (b) 15.6059; (c) 15.1754; (d) 16.0546.

Then, by (C.1a)–(C.1c) and Lemma 3.4, we can deduce that

$$
\left\| J_{A_1/\mu_1}\left(\Lambda_1\overline{u} + \overline{d}_1\right) - J_{A_1/\mu_1}\left(\Lambda_1 u^{n-1} + d_1^{n-1}\right) \right\|_{L^2}^2 + \left\| \mu_1\left(\overline{d}_1 - d_1^n\right) \right\|_{L^2}^2
$$
$$
\leq \left\| \Lambda_1\left(\overline{u} - u^{n-1}\right) + \left(\overline{d}_1 - d_1^{n-1}\right) \right\|_{L^2}^2,
$$

$$\left\|J_{A_2/\mu_2}\left(\Lambda_2\overline{u}+\overline{d}_2\right)-J_{A_2/\mu_2}\left(\Lambda_2 u^{n-1}+d_2^{n-1}\right)\right\|_{L^2}^2+\left\|\mu_2\left(\overline{d}_2-d_2^n\right)\right\|_{L^2}^2$$

$$\leq\left\|\Lambda_2\left(\overline{u}-u^{n-1}\right)+\left(\overline{d}_2-d_2^{n-1}\right)\right\|_{L^2}^2.$$

(C.2)

Combine (C.2) and (C.3) with

$$\left(\Lambda_1\left(\overline{u}-u^{n-1}\right),\mu_1\left(\overline{d}_1-d_1^{n-1}\right)\right)+\left(\Lambda_2\left(\overline{u}-u^{n-1}\right),\mu_2\left(\overline{d}_2-d_2^{n-1}\right)\right)$$

$$=-\frac{1}{\theta}\left\|\overline{u}-u^{n-1}\right\|_{L^2}^2\leq-\frac{1}{2\theta\|\Lambda_1\|^2}\left\|\Lambda_1\left(\overline{u}-u^{n-1}\right)\right\|_{L^2}^2-\frac{1}{2\theta\|\Lambda_2\|^2}\left\|\Lambda_2\left(\overline{u}-u^{n-1}\right)\right\|_{L^2}^2,$$

(C.3)

which implies that

$$\mu_1\left\|J_{A_1/\mu_1}\left(\Lambda_1\overline{u}+\overline{d}_1\right)-J_{A_1/\mu_1}\left(\Lambda_1 u^{n-1}+d_1^{n-1}\right)\right\|_{L^2}^2+\mu_1\left\|\mu_1\left(\overline{d}_1-d_1^n\right)\right\|_{L^2}^2$$

$$+\mu_2\left\|J_{A_2/\mu_2}\left(\Lambda_2\overline{u}+\overline{d}_2\right)-J_{A_2/\mu_2}\left(\Lambda_2 u^{n-1}+d_2^{n-1}\right)\right\|_{L^2}^2+\mu_2\left\|\mu_2\left(\overline{d}_2-d_2^n\right)\right\|_{L^2}^2$$

$$\leq\left(\mu_1-\frac{1}{\theta\|\Lambda_1\|^2}\right)\left\|\Lambda_1\left(\overline{u}-u^{n-1}\right)\right\|_{L^2}^2+\mu_1\left\|\overline{d}_1-d_1^{n-1}\right\|_{L^2}^2$$

$$+\left(\mu_2-\frac{1}{\theta\|\Lambda_2\|^2}\right)\left\|\Lambda_2\left(\overline{u}-u^{n-1}\right)\right\|_{L^2}^2+\mu_2\left\|\overline{d}_2-d_2^{n-1}\right\|_{L^2}^2.$$

(C.4)

Since $\mu_1\leq 1/\theta\|\Lambda_1\|^2$ and $\mu_2\leq 1/\theta\|\Lambda_2\|^2$, by (C.3) we eventually get

$$\left\|\overline{d}_1-d_1^n\right\|_{L^2}\leq\left\|\overline{d}_1-d_1^{n-1}\right\|_{L^2},\qquad\left\|\overline{d}_2-d_2^n\right\|_{L^2}\leq\left\|\overline{d}_2-d_2^{n-1}\right\|_{L^2}$$

(C.5)

as long as $u^n\neq\overline{u}$ and

$$\lim_{n\to\infty}\left\|u^{n-1}-\overline{u}\right\|_{L^2}=0.$$

(C.6)

Furthermore, by (C.4) we also get

$$\lim_{n\to\infty}\left\|J_{A_1/\mu_1}\left(\Lambda_1\overline{u}+\overline{d}_1\right)-J_{A_1/\mu_1}\left(\Lambda_1 u^{n-1}+d_1^{n-1}\right)\right\|_{L^2}=0,$$

$$\lim_{n\to\infty}\left\|J_{A_2/\mu_2}\left(\Lambda_1\overline{u}+\overline{d}_2\right)-J_{A_2/\mu_2}\left(\Lambda_2 u^{n-1}+d_2^{n-1}\right)\right\|_{L^2}=0.$$

(C.7)

Based on (C.1a) and (C.1b), using the definitions of resolvent and the Yosida approximation, it is easy to find that

$$\lim_{n\to\infty}\left\|d_1^n-d_1^{n-1}\right\|_{L^2}=0,\qquad\lim_{n\to\infty}\left\|d_2^n-d_2^{n-1}\right\|_{L^2}=0.$$

(C.8)

Then, using Corollary 4 in page 199 of [53], we can deduce that $\lim_{n\to\infty} d_1^n = \overline{d}_1$ and $\lim_{n\to\infty} d_2^n = \overline{d}_2$.

On the other hand, if $(\overline{d}_1, \overline{d}_2, \overline{u})$ is the limit of the sequence $\{(d_1^n, d_2^n, u^n)\}$ generated by Algorithm 3.3, it is easy to find that (3.13) can be rewritten as

$$
\begin{aligned}
\overline{d}_1 &= \mathrm{prox}_{\mu_1} h_1^* \left(\Lambda_1 \overline{u} + \overline{d}_1 \right), \\
\overline{d}_2 &= \mathrm{prox}_{\mu_2} h_2^* \left(\Lambda_2 \overline{u} + \overline{d}_2 \right), \\
\overline{u} &= f - \left(\frac{\mu_1}{\theta} \Lambda_1^* \overline{d}_1 + \frac{\mu_2}{\theta} \Lambda_2^* \overline{d}_2 \right)
\end{aligned}
\tag{C.9}
$$

as $n \to +\infty$. Using the relationship (2.9) in Remark 2.8, (C.1a)–(C.1c) can be then rewritten as

$$
\Lambda_1 \overline{u} = \mathrm{prox}_{1/\mu_1} h_1 \left(\Lambda_1 \overline{u} + \overline{d}_1 \right), \tag{C.10a}
$$

$$
\Lambda_2 \overline{u} = \mathrm{prox}_{1/\mu_2} h_2 \left(\Lambda_2 \overline{u} + \overline{d}_2 \right), \tag{C.10b}
$$

$$
\overline{u} = f - \left(\frac{\mu_1}{\theta} \Lambda_1^* \overline{d}_1 + \frac{\mu_2}{\theta} \Lambda_2^* \overline{d}_2 \right). \tag{C.10c}
$$

Following from (C.10a) and (C.10b), we can find that

$$
\begin{aligned}
\overline{d}_1 &= \frac{1}{\mu_1} \partial h_1 (\Lambda_1 (\overline{u})), \\
\overline{d}_2 &= \frac{1}{\mu_2} \partial h_2 (\Lambda_2 (\overline{u})).
\end{aligned}
\tag{C.11}
$$

Submitting (C.10a)–(C.10c) into (C.11), we have

$$
\theta (\overline{u} - f) + \Lambda_1^* \partial h_1 (\Lambda_1 (\overline{u})) + \Lambda_2^* \partial h_2 (\Lambda_2 (\overline{u})) = 0, \tag{C.12}
$$

which implies that $\overline{u}$ is the solution of (1.8). □

D. Proof of Theorem 4.9

Proof. From the assumption, the functional $\mathcal{M}(u, z)$ exists in at least a minimized point denoted by $(\overline{u}, \overline{z})$, which implies that $(\overline{u}, \overline{z})$ satisfies

$$
\begin{aligned}
\overline{z} &= \mathcal{F}(\overline{u}), \\
\overline{u} &= \mathcal{G}(\overline{z}).
\end{aligned}
\tag{D.1}
$$

That is to say that $\overline{u}$ is a fixed point of the operator $\mathcal{G} \circ \mathcal{F}$.

Now we show that the sequence $\{u^n\}$ generated by (4.11a)-(4.11b) converges to this fixed point $\overline{u}$. In fact, based on the nonexpansive operators $\mathcal{F}$ and $\mathcal{G}$, for the sequence $\{u^n\}$ we can get

$$\left\| u^{n+1} - \overline{u} \right\|_{L^2} = \| \mathcal{F} \circ \mathcal{G}(u^n) - \mathcal{F} \circ \mathcal{G}(\overline{u}) \|_{L^2} \leq \| u^n - \overline{u} \|_{L^2}. \tag{D.2}$$

This implies that the positive sequence $\{\| u^n - \overline{u} \|_{L^2}\}$ is monotonically decreasing. So we can find a subsequence $\{u^{n_k}\}$ from $\{u^n\}$ converging to a limit point u^* as $n \to \infty$. Form the continuity of $\mathcal{F}$ and $\mathcal{G}$, we then have

$$\| u^* - \overline{u} \|_{L^2} = \| \mathcal{F} \circ \mathcal{G}(u^*) - \overline{u} \|_{L^2}. \tag{D.3}$$

Furthermore, we can get $\overline{u} = u^*$ based on the uniqueness of the fixed point. Thus, (u^*, z^*) is the solution of (4.11a)-(4.11b), where z^* corresponds to u^*. Setting $J(u) = \int_\Omega |(1 - g)\nabla u| dx + \int_\Omega |g\nabla^2 u| dx$, we can get

$$0 = \beta(z^* - u^*) + h'(z^*),$$
$$0 \in \beta(u^* - z^*) + \partial J(u^*), \tag{D.4}$$

which implies that

$$h'(z^*) + \partial J(u^*) = 0. \tag{D.5}$$

Then u^* is the solution of (4.13) when $u^* = z^*$. $\qquad\qquad\qquad\qquad\qquad\qquad\qquad\square$

Acknowledgments

References

[1] G. Aubert and P. Kornprobst, *Mathematical Problems in Image Processing*, Springer, New York, NY, USA, 2002.

[2] T. F. Chan and J. Shen, *Image Processing and Analysis*, Society for Industrial and Applied Mathematics (SIAM), Philadelphia, Pa, USA, 2005.

[3] N. Paragios, Y. Chen, and O. Faugeras, *The Handbook of Mathematical Models in Computer Vision*, Springer, New York, NY, USA, 2006.

[4] H. W. Engl, M. Hanke, and A. Neubauer, *Regularization of Inverse Problems*, vol. 375, Kluwer Academic Publishers Group, Dordrecht, The Netherlands, 1996.

[5] L. Rudin, S. Osher, and E. Fatemi, "Nonlinear total variation based noise removal algorithms," *Physica D*, vol. 60, pp. 259–268, 1992.

[6] L. Rudin and S. Osher, "Total variation based image restoration with free local constraints," *IEEE International Conference on Image Processing*, vol. 1, no. 13–16, pp. 31–35, 1994.

[7] T. F. Chan and J. Shen, "Variational image inpainting," *Communications on Pure and Applied Mathematics*, vol. 58, no. 5, pp. 579–619, 2005.

[8] R. Wagner, S. Smith, J. Sandrik, and H. Lopez, "Statistics of speckle in ultrasound B-scans," *Transactions on Sonics Ultrasonics*, vol. 30, no. 3, pp. 156–163, 1983.

[9] G. Aubert and J.-F. Aujol, "A variational approach to removing multiplicative noise," *SIAM Journal on Applied Mathematics*, vol. 68, no. 4, pp. 925–946, 2008.

[10] A. Montillo, J. Udupa, L. Axel, and D. Metaxas, "Interaction between noise suppression and inhomogeneity correction in MRI," in *Medical Imaging, Image Processing*, vol. 5032 of *Proceedings of SPIE*, pp. 1025–1036, 2003.

[11] Y.-M. Huang, M. K. Ng, and Y.-W. Wen, "A new total variation method for multiplicative noise removal," *SIAM Journal on Imaging Sciences*, vol. 2, no. 1, pp. 20–40, 2009.

[12] T. Chan, A. Marquina, and P. Mulet, "High-order total variation-based image restoration," *SIAM Journal on Scientific Computing*, vol. 22, no. 2, pp. 503–516, 2000.

[13] M. Lysaker, A. Lundervold, and X. Tai, "Noise removal using fourth-order partial differential equation with applications to medical magnetic resonance images in space and time," *IEEE Transactions on Image Processing*, vol. 12, no. 12, pp. 1579–1590, 2003.

[14] O. Scherzer, "Denoising with higher order derivatives of bounded variation and an application to parameter estimation," *Computing. Archives for Scientific Computing*, vol. 60, no. 1, pp. 1–27, 1998.

[15] Y.-L. You and M. Kaveh, "Fourth-order partial differential equations for noise removal," *IEEE Transactions on Image Processing*, vol. 9, no. 10, pp. 1723–1730, 2000.

[16] F. Li, C. Shen, J. Fan, and C. Shen, "Image restoration combining a total variational filter and a fourth-order filter," *Journal of Visual Communication and Image Representation*, vol. 18, no. 4, pp. 322–330, 2007.

[17] A. Chambolle, "An algorithm for total variation minimization and applications," *Journal of Mathematical Imaging and Vision*, vol. 20, no. 1-2, pp. 89–97, 2004.

[18] A. Chambolle, "Total variation minimization and a class of binary MRF models," in *Workshop on Energy Minimization Methods in Computer Vision and Pattern Recognition (EMMCVPR '05)*, pp. 136–152, 2005.

[19] A. Chambolle and T. Pock, "A first-order primal-dual algorithm for convex problems with applications to imaging," *Journal of Mathematical Imaging and Vision*, vol. 40, no. 1, pp. 120–145, 2011.

[20] E. Esser, X. Zhang, and T. F. Chan, "A general framework for a class of first order primal-dual algorithms for convex optimization in imaging science," *SIAM Journal on Imaging Sciences*, vol. 3, no. 4, pp. 1015–1046, 2010.

[21] M. Zhu, S. J. Wright, and T. F. Chan, "Duality-based algorithms for total-variation-regularized image restoration," *Computational Optimization and Applications*, vol. 47, no. 3, pp. 377–400, 2010.

[22] D. Goldfarb and W. Yin, "Second-order cone programming methods for total variation-based image restoration," *SIAM Journal on Scientific Computing*, vol. 27, no. 2, pp. 622–645, 2005.

[23] K. Chen and X.-C. Tai, "A nonlinear multigrid method for total variation minimization from image restoration," *Journal of Scientific Computing*, vol. 33, no. 2, pp. 115–138, 2007.

[24] J.-F. Cai, S. Osher, and Z. Shen, "Split Bregman methods and frame based image restoration," *Multiscale Modeling & Simulation*, vol. 8, no. 2, pp. 337–369, 2009.

[25] T. Goldstein and S. Osher, "The split Bregman method for L1-regularized problems," *SIAM Journal on Imaging Sciences*, vol. 2, no. 2, pp. 323–343, 2009.

[26] C. A. Micchelli, L. X. Shen, and Y. S. Xu, "Proximity algorithms for image models: denoising," *Inverse Problems*, vol. 27, no. 4, 2011.

[27] M. Burger, K. Frick, S. Osher, and O. Scherzer, "Inverse total variation flow," *Multiscale Modeling & Simulation*, vol. 6, no. 2, pp. 366–395, 2007.

[28] M. Afonso and J. Bioucas-Dias, *Image Restoration with Compound Regularization Using a Bregman Iterative Algorithm. Signal Processing with Adaptive Sparse Structured Representations*, 2009.

[29] X. C. Tai and C. Wu. Augmented, "Lagrangian method, dual methods and split Bregman iteration for ROF model," in *Proceedings of the Second International Conference on Scale Space and Variational Methods in Computer Vision (SSVMCV '09)*, vol. 5567, pp. 502–513, 2009.

[30] C. Chen, B. He, and X. Yuan, "Matrix completion via an alternating direction method," *IMA Journal of Numerical Analysis*, vol. 32, no. 1, pp. 227–245, 2012.

[31] J. Yang and Y. Zhang, "Alternating direction algorithms for ℓ_1-problems in compressive sensing," *SIAM Journal on Scientific Computing*, vol. 33, no. 1, pp. C250–C278, 2011.

[32] R. H. Chan, J. Yang, and X. Yuan, "Alternating direction method for image inpainting in wavelet domains," *SIAM Journal on Imaging Sciences*, vol. 4, no. 3, pp. C807–C826, 2011.

[33] J. Yang and X. Yuan, "Linearized augmented Lagrangian and alternating direction methods for nuclear norm minimization," *Mathematics of Computation*, vol. 82, pp. 301–329, 2013.

[34] R. Glowinski and P. Le Tallec, *Augmented Lagrangian and Operator-Splitting Methods in Nonlinear Mechanics*, vol. 9, Society for Industrial and Applied Mathematics (SIAM), 1989.

[35] R. T. Rockafellar, *Convex Analysis*, Princeton University Press, Princeton, NJ, USA, 1970.

[36] L. Ambrosio, N. Fusco, and D. Pallara, *Functions of Bounded Variation and Free Discontinuity Problems*, Oxford University Press, New York, NY, USA, 2000.

[37] H. Attouch, G. Buttazzo, and G. Michaille, *Variational Analysis in Sobolev and BV Spaces: Applications to PDEs and Optimization*, vol. 6, Society for Industrial and Applied Mathematics (SIAM), Philadelphia, Pa, USA, 2006.

[38] J. Aubin and H. Frankowska, *Set-Valued Analysis*, Springer, 1990.

[39] A. Bermúdez and C. Moreno, "Duality methods for solving variational inequalities," *Computers & Mathematics with Applications*, vol. 7, no. 1, pp. 43–58, 1981.

[40] C. L. Byrne, *Applied Iterative Methods*, A K Peters, 2008.

[41] L. C. Evans and R. F. Gariepy, *Measure Theory and Fine Properties of Functions*, CRC Press, Boca Raton, Fla, USA, 1992.

[42] I. Ekeland and R. Teman, *Convex Analysis and Variational Problems. North-Holland*, Amsterdam, The Netherlands, 1976.

[43] Y. Meyer, *Oscillating Patterns in Image Processing and Nonlinear Evolution Equations*, University Lecture Series, American Mathematical Society, 2001.

[44] Y. Wang, J. Yang, W. Yin, and Y. Zhang, "A new alternating minimization algorithm for total variation image reconstruction," *SIAM Journal on Imaging Sciences*, vol. 1, no. 3, pp. 248–272, 2008.

[45] A. Marquina and S. J. Osher, "Image super-resolution by TV-regularization and Bregman iteration," *Journal of Scientific Computing*, vol. 37, no. 3, pp. 367–382, 2008.

[46] S. Setzer, "Split Bregman algorithm, Douglas-Rachford splitting and frame shrinkage," in *Proceedings of the Second International Conference on Scale Space and Variational Methods in Computer Vision (SSVMCV '09)*, vol. 5567, pp. 464–476, 2009.

[47] D. Gabay and B. Mercier, "A dual algorithm for the solution of nonlinear variational problems via finite-element approximations," *Computers and Mathematics with Applications*, vol. 2, no. 1, pp. 17–40, 1976.

[48] D. Bertsekas, *Constrained Optimization and Lagrange Multiplier Methods*, Athena Scientific, 1996.

[49] E. Esser, "Applications of the Lagrangian-based alternating direction methods and connections to split Bregman," UCLA Report 2009-31.

[50] P. L. Combettes and V. R. Wajs, "Signal recovery by proximal forward-backward splitting," *Multiscale Modeling & Simulation*, vol. 4, no. 4, pp. 1168–1200, 2005.

[51] A. Beck and M. Teboulle, "A fast iterative shrinkage-thresholding algorithm for linear inverse problems," *SIAM Journal on Imaging Sciences*, vol. 2, no. 1, pp. 183–202, 2009.

[52] Y. Nesterov, "A method for unconstrained convex minimization problem with the rate of convergence $O(1/k^2)$," *Soviet Mathematics Doklady*, vol. 27, no. 2, pp. 372–376, 1983.

[53] A. Pazy, "On the asymptotic behavior of iterates of nonexpansive mappings in Hilbert space," *Israel Journal of Mathematics*, vol. 26, no. 2, pp. 197–204, 1977.